Long-time evolution of pulses in the Korteweg–de Vries equation in the absence of solitons reexamined: Whitham method

M. Isoard,[1] A. M. Kamchatnov,[2,3] and N. Pavloff[1]
[1]*LPTMS, CNRS, Univ. Paris-Sud, Université Paris-Saclay, 91405 Orsay, France*
[2]*Institute of Spectroscopy, Russian Academy of Sciences, Troitsk, Moscow, 108840, Russia*
[3]*Moscow Institute of Physics and Technology, Institutsky lane 9, Dolgoprudny, Moscow region, 141701, Russia*

(Received 12 October 2018; published 16 January 2019)

We consider the long-time evolution of pulses in the Korteweg–de Vries equation theory for initial distributions which produce no soliton but instead lead to the formation of a dispersive shock wave and of a rarefaction wave. An approach based on Whitham modulation theory makes it possible to obtain an analytic description of the structure and to describe its self-similar behavior near the soliton edge of the shock. The results are compared with numerical simulations.

DOI: 10.1103/PhysRevE.99.012210

I. INTRODUCTION

It is well known that pulses propagating through a nonlinear medium typically experience wave breaking. Their long-time evolution depends on which effect—in addition to the nonlinearity—dominates after the wave breaking moment: viscosity or dispersion. If viscosity dominates, then the shock corresponds to a region of localized extend in which the slow variables display a sharp transition. A typical small-amplitude viscous shock can be modeled by the Burgers' equation

$$u_t + uu_x = \nu u_{xx}, \tag{1}$$

for which a full analytic theory has been developed (see, e.g., Ref. [1]). For a positive initial profile $u(x, t = 0) \equiv u_0(x) > 0$ which is well-enough localized [i.e., $u_0(x) \to 0$ fast enough for $|x| \to \infty$] the time-evolved pulse acquires a triangle-like shape at its front edge [or at its rear edge if $u_0(x) < 0$[1]], gradually spreading out with decreasing amplitude.

The situation changes drastically if dispersive effects dominate rather than viscosity. In this case the typical evolution can be described by the celebrated Korteweg–de Vries (KdV) equation

$$u_t + 6uu_x + u_{xxx} = 0, \tag{2}$$

which admits oscillating solutions ranging from linear waves to bright solitons. A positive localized initial pulse $u_0(x) > 0$, after an intermediate stage of wave breaking and complicated deformation, eventually evolves into a sequence of solitons with some amount of linear dispersive waves. The characteristics of the solitons are determined by the initial distribution $u_0(x)$. If this initial pulse is intense enough—so that the number of solitons is large—one may determine the parameters of these solitons by means of the asymptotic formula of Karpman [2] which is obtained in the framework of the inverse scattering transform method discovered by Gardner, Green, Kruskal, and Miura [3]. However, if $u_0(x) < 0$, since Eq. (2) does not admit dark (i.e., "negative") solitons, then wave breaking does not result in the production of solitons, but it rather leads to the formation of a dispersive shock wave (DSW) connected to a triangle-like rarefaction wave which is the remnant of the initial trough. The shape and the time evolution of this oscillatory structure are highly nontrivial and considerable efforts have been invested in their study.

In an early investigation of Berezin and Karpman [4] it was shown that the KdV equation admits solutions of the form

$$u(x, t) = \frac{1}{t^{2/3}} f\left(\frac{x}{t^{1/3}}\right), \tag{3}$$

and numerical simulations of these authors demonstrated that some region of the evolving wave structure is indeed described by solutions of type (3). The existence of such a region was confirmed by the inverse scattering transform method in Refs. [5,6] and its "quasi-linear" part was studied in Ref. [7]. An extensive study of the asymptotic evolution of the pulse in the absence of solitons was performed in Ref. [8] where different characteristic parts of the wave structure were distinguished and their main parameters were calculated. However, in this reference, Ablowitz and Segur—who first explicitly point to the formation of a dispersive shock wave—confined themselves to the analytic study of typical limiting cases and explicit formulas for the whole dispersive shock wave region were found much later [9] with the use of a quite involved analysis of the associated Riemann-Hilbert problem. This approach was developed further in Refs. [10–12] and other papers.

Although the above-mentioned approaches are mathematically strict, the methods used are difficult and the theory developed has not found applications to concrete problems related with other integrable evolution equations. Since the question of evolution of pulses in the absence of solitons is related with experiments in physics of water waves [13,14], Bose-Einstein condensates [15,16], and nonlinear optics [17,18], the development of a simpler and more transparent physically approach is desirable. Such an approach, based on the Whitham theory

[1]A so-called N-wave appears if $u_0(x)$ has both polarities; see, e.g., Ref. [1].

of modulations of nonlinear waves [19], was suggested long ago by Gurevich and Pitaevskii [20] and since that time it has developed into a powerful method with numerous applications (see, e.g., the review article [21]). Despite the facts that some elements of the Whitham theory were used in Refs. [6,8] and that the general solution of the solitonless initial value problem has been obtained in Ref. [22], no asymptotic analysis has been performed within Whitham's formalism, so that its relationship with the previous results remained unclear.

The main goal of the present paper is to fill this gap and to apply the Whitham theory to the description of the asymptotic evolution of initial pulses in the small dispersion limit (or for wide pulses) under the condition of absence of solitons. We show that the combination of two ideas—self-similarity of the solution and quasisimple character [23] of the dispersive shock wave—permits an asymptotic analysis of the solution. The relatively simple theory developed in the present work should be useful in the analysis of experiments devoted to the evolution of pulses of this type.

The paper is organized as follows. In Sec. II we present the main aspects of Whitham theory and of the generalized hodograph method applying to quasisimple waves (following Refs. [22–28]). In Sec. III, the application of the ideas of Ref. [23] to the soliton edge of the DSW makes it possible to find the law of motion of this edge and suggests a self-similar asymptotic behavior consistent with Eq. (3). In Sec. IV we perform the large-time asymptotic analysis of the rear (soliton) part of the dispersive shock wave by the Whitham method within this self-similarity assumption. This yields a surprisingly simple derivation of the solution first explicitly obtained in Ref. [9]. The description of the DSW in its full range by the method of El and Khodorovskii [22] is presented in a self-contained manner in Sec. V. In this section we consider the time evolution of several initial profiles illustrating the possible different behaviors in the shock region and compare the theoretical results with numerical simulations. We present our conclusions in Sec. VI.

II. WHITHAM THEORY AND THE GENERALIZED HODOGRAPH METHOD

A. The smooth part of the profile

We consider an initial pulse with nonpositive profile $u(x, t = 0) = u_0(x)$ defined on finite interval of x and having a single minimum $\min_{x\in\mathbb{R}}\{u_0(x)\} = -1$ (this value can be changed by an appropriate rescaling on u, x, and t). We consider a initial profile of finite extend x_0, and assume that $x_0 \gg 1$, so that in a first stage of evolution one can neglect dispersive effects. This amounts to replace the KdV dynamics by the Hopf equation,

$$r_t + 6\,r\,r_x = 0. \tag{4}$$

We changed notation here to mark the difference between $r(x, t)$, solution of the approximate equation (4), and $u(x, t)$, which is the exact solution of the KdV equation (2). The solution of the Hopf equation is well known (see, e.g., Ref. [29]) and it is given in implicit form in terms of functions inverse to $u_0(x)$, as explained now.

In the case we consider, $u_0(x)$ has a single minimum and its inverse function is two valued. We denote its two branches

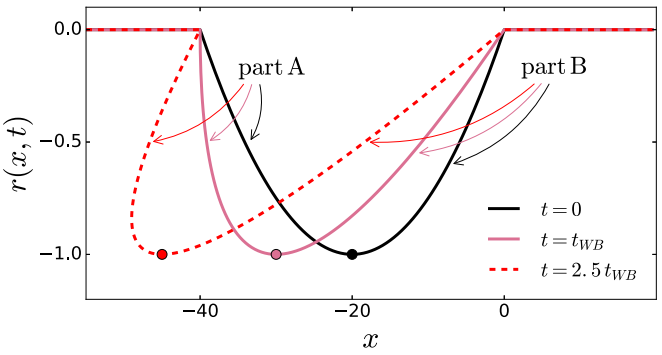

FIG. 1. The solid black, solid pink, and dashed red lines represent $r(x, t)$ solution of (4) for times $t = 0$, $t = t_{\rm WB}$, and $t = 2.5\,t_{\rm WB}$ for an initial condition $r(x, 0)$ given by the parabolic profile $u_0(x)$ defined in Eq. (6) with $x_0 = 40$. The dots represent the position of the minimum $\min_{x\in\mathbb{R}}\{r(x, t)\}$ which separates parts A (at the left) and B (at the right) of the profile.

as $w^{\rm A}(r)$ and $w^{\rm B}(r)$, where the first function refers to the part of the pulse to the left of its minimum and the second one to its right. Then the solution of the Hopf equation is given by the formulas

$$x - 6\,r\,t = w^{\rm A}(r), \tag{5a}$$

$$x - 6\,r\,t = w^{\rm B}(r). \tag{5b}$$

For example, in case of a parabolic initial pulse

$$u_0(x) = \begin{cases} 4\,x(x + x_0)/x_0^2 & \text{for } -x_0 \leqslant x \leqslant 0, \\ 0 & \text{elsewhere,} \end{cases} \tag{6}$$

the inverse functions are equal to

$$\begin{aligned} w^{\rm A}(r) &= \tfrac{x_0}{2}(-1 - \sqrt{1 + r}\,), \\ w^{\rm B}(r) &= \tfrac{x_0}{2}(-1 + \sqrt{1 + r}\,), \end{aligned} \qquad \text{where } r \in [-1, 0]. \tag{7}$$

Figure 1 represents the initial profile (6) and its time evolution as computed from Eqs. (5), i.e., without taking dispersive effects into account. Figure 2 represents the corresponding functions $w^{\rm A}(r)$ and $w^{\rm B}(r)$. In the following we shall perform the explicit computations using this initial profile. Other types

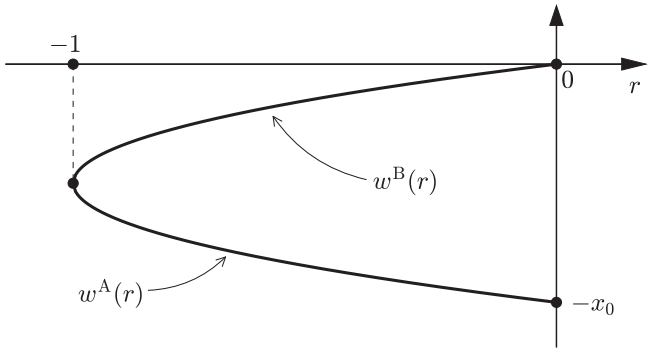

FIG. 2. The two branches $w^{\rm A}(r)$ and $w^{\rm B}(r)$ of the reciprocal function of $u_0(x)$. The figure is drawn for the initial parabolic profile (6) [the corresponding expressions of $w^{\rm A}(r)$ and $w^{\rm B}(r)$ are given in Eq. (7)] but the behavior is the generic one.

of profiles, with less generic behaviors, will be presented and discussed in Sec. V.

The wave-breaking time is the time $t_{\rm WB} = 1/\max(-6\,du_0/dx)$ at which the solution of (4) becomes infinitely steep (see, e.g., Ref. [1]). In the present work we consider initial profiles for which the largest slope $\max(-du_0/dx)$ is reached at $x = -x_0$ for $r = 0$ and thus

$$t_{\rm WB} = -\frac{1}{6}\left(\frac{dw^{\rm A}}{dr}\right)_{r=0}. \tag{8}$$

For the initial profile (6) we get $t_{\rm WB} = x_0/24$. For $t \geqslant t_{\rm WB}$ the dispersionless approximation fails (the corresponding formal solution of the Hopf equation is multivalued), and a DSW is formed, initially around $x = -x_0$, which then expands toward the negative x direction. We now explain how it can be described within Whitham modulational theory.

B. Periodic solutions and their modulations

The KdV equation (2) admits nonlinear periodic solutions which can be written in terms of three parameters $r_1 \leqslant r_2 \leqslant r_3$ as (see, e.g., Ref. [29])

$$u(x,t) = r_3 + r_2 - r_1 - 2(r_2 - r_1) \times \mathrm{sn}^2(\sqrt{r_3 - r_1}(x - Vt), m), \tag{9}$$

where

$$V = 2(r_1 + r_2 + r_3) \tag{10}$$

and

$$m = \frac{r_2 - r_1}{r_3 - r_1}. \tag{11}$$

The notation "sn" in formula (9) refers to the Jacobi sine function (see, e.g., Ref. [30]). For constant parameters r_i expression (9) is an exact (single phase) solution of the KdV equation, periodic in time and space with wavelength

$$L = \frac{2K(m)}{\sqrt{r_3 - r_1}}, \tag{12}$$

where $K(m)$ is the complete elliptic integral of the first kind.

According to the Gurevich-Pitaevskii scheme, a DSW may be described as a modulated nonlinear periodic wave of type (9) for which the r_i's slowly depend on time and position and evolve according to the Whitham equations (see, e.g, Refs. [21,29])

$$\partial_t r_i + v_i(r_1, r_2, r_3)\partial_x r_i = 0, \quad i = 1, 2, 3. \tag{13}$$

The quantities v_i in these equations are the Whitham velocities. Their explicit expressions have first been derived by Whitham [19] and can also be obtained from the relation

$$v_i = \left(1 - \frac{L}{\partial_i L}\,\partial_i\right)V = V - 2\,\frac{L}{\partial_i L}, \tag{14}$$

where L is the wavelength (12), V the phase velocity (10) of the nonlinear periodic solution (9), and ∂_i stands for ∂_{r_i}. One gets

$$\begin{aligned} v_1 &= 2(r_1 + r_2 + r_3) + \frac{4(r_2 - r_1)K(m)}{E(m) - K(m)}, \\ v_2 &= 2(r_1 + r_2 + r_3) - \frac{4(r_2 - r_1)(1 - m)K(m)}{E(m) - (1 - m)K(m)}, \\ v_3 &= 2(r_1 + r_2 + r_3) + \frac{4(r_3 - r_1)(1 - m)K(m)}{E(m)}, \end{aligned} \tag{15}$$

where $E(m)$ is the complete elliptic integral of the second kind.

Since Eqs. (13) have a diagonal form (that is, they include derivatives of a single parameter r_i in each equation), the variables r_i are called Riemann invariants of the Whitham equations—Riemann was the first who introduced such variables in the theory of nonlinear waves.

The two edges of the DSW are denoted as $x_{\rm L}(t)$ and $x_{\rm R}(t)$. The first one is the small-amplitude edge; it is at the left of the DSW in the case we consider. Within the Whitham approximation, it makes contact between the DSW and the undisturbed profile: $u(x,t) = 0$ for $x \leqslant x_{\rm L}(t)$. The small-amplitude version of (9) corresponds to the limit $m \ll 1$ and takes the form

$$u(x,t) = r_3 + (r_2 - r_1)\cos[2\sqrt{r_3 - r_1}(x - Vt)]. \tag{16}$$

In this harmonic linear limit, $r_2 \to r_1$ $(m \to 0)$ and the Whitham velocities (15) reduce to

$$\begin{aligned} v_1|_{r_2=r_1} &= v_2|_{r_2=r_1} = 12\,r_1 - 6\,r_3, \\ v_3|_{r_2=r_1} &= 6\,r_3. \end{aligned} \tag{17}$$

Around the left boundary of the DSW, the amplitude $2(r_2 - r_1)$ of the oscillations is small and since this edge propagates along a zero background, we arrive at the conclusion that $r_3 = 0$ and $r_1 = r_2$ for $x = x_{\rm L}(t)$.

The other edge, at the right side of the DSW, is the large-amplitude soliton edge, with $m = 1$. Therefore we must have here $r_2 = r_3$ and in this limit the nonlinear pattern (9) degenerates into a soliton solution of the form

$$u(x,t) = r_1 + \frac{2(r_2 - r_1)}{\cosh^2[\sqrt{r_2 - r_1}(x - Vt)]}. \tag{18}$$

This implies that the right of the DSW is bounded by a soliton for which the Whitham velocities are given by

$$\begin{aligned} v_1|_{r_2=r_3} &= 6\,r_1, \\ v_2|_{r_2=r_3} &= v_3|_{r_2=r_3} = 2\,r_1 + 4\,r_3. \end{aligned} \tag{19}$$

C. Generalized hodograph method

The dispersionless approach of Sec. II A leads, after the wave-breaking time, to an nonphysical, multivalued solution. The form, displayed in Fig. 1, of $r(x, t \geqslant t_{\rm WB})$ in the region of multivaluedness suggests that the DSW accounting for the post wave-breaking dynamics should be described by Whitham-Riemann invariants arranged in a configuration such that $r_3 = 0$ (thus ensuring matching with the unperturbed profile at the left), whereas r_2 and r_1 both depend on x and t, with always $r_3 \geqslant r_2 \geqslant r_1$.

The contact of the DSW with the smooth profile which prevails for $x \geqslant x_{\rm R}(t)$ imposes the condition

$r_1(x_R(t),t) = r(x_R(t),t)$, where $r(x,t)$ is a solution of the Hopf equation (4) with initially $r(x,0) = u_0(x)$. Therefore the description of the DSW for $x \in [x_L(t), x_R(t)]$ imposes the boundary conditions

$$r_1(x_R(t),t) = r(x_R(t),t) \equiv r_R(t), \quad r_2(x_R(t),t) = 0, \tag{20a}$$

$$r_1(x_L(t),t) = r_2(x_L(t),t) \equiv r_L(t). \tag{20b}$$

Note that all the above functions are only defined after the wave breaking time, i.e., for $t \geqslant t_{WB}$.

This type of structure, in which two Riemann invariants (r_1 and r_2) change along the DSW, is not a simple wave solution; it belongs to the class of "quasisimple waves" introduced in Ref. [23]. In this case, Eq. (13) with $i = 3$ is trivially satisfied and for solving the remaining two Whitham equations we use the so-called generalized hodograph method of Tsarev [31]. To this end, one introduces two functions $W_i(r_1, r_2)$ ($i = 1$ or 2), making it possible to write a vector generalization of Eq. (5) for the Whitham system:

$$x - v_i(r_1, r_2)t = W_i(r_1, r_2), \quad i = 1, 2. \tag{21}$$

For the sake of brevity we have noted in the above equation $v_i(r_1, r_2) = v_i(r_1, r_2, r_3 = 0)$ for $i \in \{1, 2\}$; we will keep this notation henceforth. The W_i's must satisfy the compatibility equation found by substituting (21) into (13). This leads to the Tsarev equations:

$$\frac{\partial_j W_i}{W_i - W_j} = \frac{\partial_j v_i}{v_i - v_j}, \text{ for } i \neq j. \tag{22}$$

One can show (see, e.g., Refs. [25,27,28]) that (22) is solved for W_i's of the form

$$W_i = \left(1 - \frac{L}{\partial_i L}\partial_i\right)\mathscr{W} = \mathscr{W} + \left(\frac{1}{2}v_i - r_1 - r_2\right)\partial_i \mathscr{W}, \tag{23}$$

where $\mathscr{W}(r_1, r_2)$ is solution of the Euler-Poisson equation

$$\partial_{12}\mathscr{W} = \frac{\partial_1 \mathscr{W} - \partial_2 \mathscr{W}}{2(r_1 - r_2)}. \tag{24}$$

There is, however, a subtle point here, which was first understood in Ref. [23] (see also Ref. [22]). After the wave breaking time, the development of the dispersive shock wave occurs in *two* steps:

(A) Initially (when t is close to t_{WB}), the DSW is connected at its right edge to the smooth profile coming from the time evolution of part A of the initial profile. In this case, for a given time t, the lower value of $u(x,t)$ is reached within the smooth part of the profile and keeps its initial values (-1).

(B) Then, after a while, the left part of the initial profile (part A) has been "swallowed" by the DSW which is then connected at its right to the smooth profile coming from the time evolution of part B of $u_0(x)$. In this case, the minimum $\min_{x\in\mathbb{R}}\{u(x,t)\}$ is reached inside the DSW (or at its boundary), is negative and larger than -1 (i.e., less pronounced than in the previous case A), and asymptotically tends to 0 for large time.

We denote the region of the DSW [and of the (x,t) plane] in which r_1 is a decreasing function of x as region A, the part where it increases as region B. In region A of the (x,t) plane, we denote by $\mathscr{W}^A(r_1, r_2)$ the solution of the Euler-Poisson equation; in region B we denote it instead as $\mathscr{W}^B(r_1, r_2)$. These two forms are joined by the line $r_1 = -1$ (cf. the upper plots of Fig. 5) along which

$$\mathscr{W}^A(-1, r_2) = \mathscr{W}^B(-1, r_2). \tag{25}$$

Since the general solution of the Euler-Poisson equation with the appropriate boundary conditions, and the construction of the resulting nonlinear pattern are quite involved, we shall first consider some particular—but useful—results which follow from general principles of the Whitham theory.

III. MOTION OF THE SOLITON EDGE OF THE SHOCK

During the first stage of evolution of the DSW, its right (solitonic) edge is connected to the smooth dispersionless solution described by formula (5a), that is we have here

$$x_R - 6r_R t = w^A(r_R). \tag{26}$$

On the side of the DSW, in vicinity of this boundary, the Whitham equations (13) with the limiting expressions (19) (where $r_3 = 0$) for the velocities v_i are given by

$$\partial_t r_1 + 6r_1\partial_x r_1 = 0, \qquad \partial_t r_2 + 2r_1\partial_x r_2 = 0. \tag{27}$$

For solving these equations one can perform a classical hodograph transformation (see, e.g., Ref. [29]), that is, one assume that x and t are functions of the independent variables r_1 and r_2: $t = t(r_1, r_2)$, $x = x(r_1, r_2)$. We find from Eqs. (27) that these functions must satisfy the linear system

$$\frac{\partial x}{\partial r_1} - 2r_1\frac{\partial t}{\partial r_1} = 0, \qquad \frac{\partial x}{\partial r_2} - 6r_1\frac{\partial t}{\partial r_2} = 0.$$

At the boundary with the dispersionless solution [where $r_1 = r_R$, see (20a)] the first equation reads

$$\frac{\partial x_R}{\partial r_R} - 2\,r_R\frac{\partial t}{\partial r_R} = 0, \tag{28}$$

and this must be compatible with Eq. (26). Differentiation of Eq. (26) with respect to r_R and elimination of $\partial x_R/\partial r_R$ with the use of Eq. (28) yield the differential equation for the function $t(r_R) \equiv t(r_R, 0)$:

$$4\,r_R\frac{dt}{dr_R} + 6\,t = -\frac{dw^A(r_R)}{dr_R}. \tag{29}$$

At the wave-breaking time, $r_R = 0$, and (29) gives the correct definition (8) of the wave-breaking time: $t_{WB} = t(0)$. Elementary integration then yields

$$\begin{aligned} t(r_R) &= \frac{1}{4(-r_R)^{3/2}}\int_0^{r_R}\sqrt{-r}\,\frac{dw^A(r)}{dr}\,dr \\ &= \frac{1}{8(-r_R)^{3/2}}\int_0^{r_R}\frac{w^A(r)}{\sqrt{-r}}dr - \frac{w^A(r_R)}{4\,r_R}. \end{aligned} \tag{30}$$

Substituting this into (26) we get the following expression for the function $x_R(r_R) \equiv x(r_R, 0)$:

$$\begin{aligned} x_R(r_R) &= -\frac{3}{2\sqrt{-r_R}}\int_0^{r_R}\sqrt{-r}\,\frac{dw^A(r)}{dr}dr + w^A(r_R) \\ &= -\frac{3}{4\sqrt{-r_R}}\int_0^{r_R}\frac{w^A(r)}{\sqrt{-r}}dr - \frac{1}{2}w^A(r_R). \end{aligned} \tag{31}$$

The two formulas (30) and (31) define in an implicit way the law of motion $x = x_{\rm R}(t)$ of the soliton edge of the DSW.

The above expressions are correct as long as the soliton edge is located inside region A, that is up to the moment

$$t_{\rm A/B} = t(-1) = \frac{1}{4}\int_0^{-1} \sqrt{-r}\,\frac{dw^{\rm A}(r)}{dr}dr, \tag{32}$$

after which the soliton edge connects with part B of the smooth profile. Concretely, for a time $t > t_{\rm A/B}$, we have to solve the differential equation

$$4\,r_{\rm R}\frac{dt}{dr_{\rm R}} + 6\,t = -\frac{dw^{\rm B}(r_{\rm R})}{dr_{\rm R}}$$

with the initial condition $t(-1) = t_{\rm A/B}$. This yields

$$t(r_{\rm R}) = \frac{1}{4(-r_{\rm R})^{3/2}}\left[\int_0^{-1}\sqrt{-r}\,\frac{dw^{\rm A}(r)}{dr}dr + \int_{-1}^{r_{\rm R}}\sqrt{-r}\,\frac{dw^{\rm B}(r)}{dr}dr\right] \tag{33}$$

and

$$x_{\rm R}(r_{\rm R}) = -\frac{3}{2(-r_{\rm R})^{1/2}}\left[\int_0^{-1}\sqrt{-r}\,\frac{dw^{\rm A}(r)}{dr}dr + \int_{-1}^{r_{\rm R}}\sqrt{-r}\,\frac{dw^{\rm B}(r)}{dr}dr\right] + w^{\rm B}(r_{\rm R}). \tag{34}$$

At asymptotically large time $t \to \infty$ one is at stage B of evolution, with furthermore $r_{\rm R} \to 0$. Hence the upper limit of integration in the second integrals of formulas (33) and (34) can be put equal to zero. Integration over r in the resulting expressions can be replaced by integration over x with account of the fact that $w^{\rm A,B}(r)$ represent two branches of the inverse function of $r = u_0(x)$, so we get

$$t(r_{\rm R}) \simeq \frac{\mathcal{A}}{4(-r_{\rm R})^{3/2}}, \quad \text{where} \quad \mathcal{A} = \int_{\mathbb{R}}\sqrt{-u_0(x)}\,dx$$

is a measure of the amplitude of the initial trough. Consequently, we obtain

$$r_{\rm R}(t) = -\left(\frac{\mathcal{A}}{4t}\right)^{2/3}, \quad x_{\rm R}(t) = -\frac{3\mathcal{A}^{2/3}}{2^{1/3}}t^{1/3}, \tag{35}$$

where we have neglected a term of order x_0 which is small compared to the infinitely increasing time-dependent ones.

At large time, the dispersionless part of the profile between $x = 0$ and $x_{\rm R}(t)$ is stretched to a quasilinear behavior $u(x,t) = x\,r_{\rm R}(t)/x_{\rm R}(t)$, and one thus has

$$\int_{x_{\rm R}(t)}^{0} dx\sqrt{-u(x,t)} = -\frac{2}{3}x_{\rm R}(t)\sqrt{-r_{\rm R}(t)} = \mathcal{A}, \tag{36}$$

which means that the quantity $\mathcal{A}$ is conserved, at least at the level of the present asymptotic analysis. This situation is reminiscent of—but different from—the dissipative case where nonlinear patterns of triangular shape may also appear at the rear edge of a (viscous) shock. In the dissipative case there also exists a conserved quantity. For Burgers' equation, for instance, with an initial condition of type (6), a single viscous shock appears which is followed by an asymptotically triangular wave. This means that the details of the initial distribution are lost (as in the present case), but for Burgers' equation the conserved quantity is not the quantity $\mathcal{A}$ defined in Eq. (36), but the integral $\int_{I(t)} dx\,u(x,t)$, where $I(t)$ is the support of the triangular wave (equivalent to our segment $[x_{\rm R}(t), 0]$).

Formulas (35) suggest that in the vicinity of the soliton edge, the behavior of the DSW must be self-similar, and we now turn to the investigation of this possibility in the framework of Whitham theory.

IV. SIMILARITY SOLUTION AT THE SOLITON EDGE OF THE SHOCK

In this section we use the Whitham approach to obtain the long-time asymptotic behavior of the shock close to $x_{\rm R}(t)$, valid up to $x \sim -t^{1/3}(\ln t)^{3/2}$ (see Refs. [8,9]).

Equations (35) suggest that, close to the soliton edge of the DSW, the Riemann invariants r_1 and r_2 have the following scaling form:

$$r_i = \frac{1}{t^{2/3}}R_i\left(\frac{x}{t^{1/3}}\right). \tag{37}$$

Here $x < 0$ and since $r_1 < r_2 < 0$, we have $R_1 < R_2 < 0$. The scaling (37) agrees with the scaling (3) of the full KdV equation first noticed in Refs. [4–6]. Written in terms of the rescaled Riemann parameters R_1 and R_2 and of the self-similar variable $z = x/t^{1/3}$, the Whitham equations (13) read

$$\frac{dR_i}{dz} = -\frac{2R_i}{z - 3R_1V_i(m)}, \qquad i = 1, 2, \tag{38}$$

where

$$m = 1 - R_2/R_1, \tag{39}$$

and the velocities $V_1(m)$ and $V_2(m)$ are given by

$$V_1(m) = 2(2-m) - \frac{4mK(m)}{E(m) - K(m)}, \qquad V_2(m) = 2(2-m) + \frac{4m(1-m)K(m)}{E(m) - (1-m)K(m)}. \tag{40}$$

The two equations (38) can be reduced to a single one if we introduce the variable

$$\zeta = z/R_1 \tag{41}$$

and look for the dependence of ζ on m. A simple calculation yields the differential equation

$$\frac{d\zeta}{dm} = \frac{[\zeta - V_1(m)][\zeta - 3V_2(m)]}{2(1-m)[V_2(m) - V_1(m)]}, \tag{42}$$

whose basic properties can be studied in the phase plane (m, ζ). The phase portrait in this plane is displayed in Fig. 3. It admits the singular points

$$\begin{array}{llll} (0,12), & (0,36) & \text{for} & m = 0; \\ (1,6), & (1,6) & \text{for} & m = 1. \end{array} \tag{43}$$

As is clear from Fig. 3, the point (0,12) is a node and the point (0,36) is a saddle. At $m = 1$ the two singular points merge into one (1,6) of a mixed saddle-node type. Numerical solution of

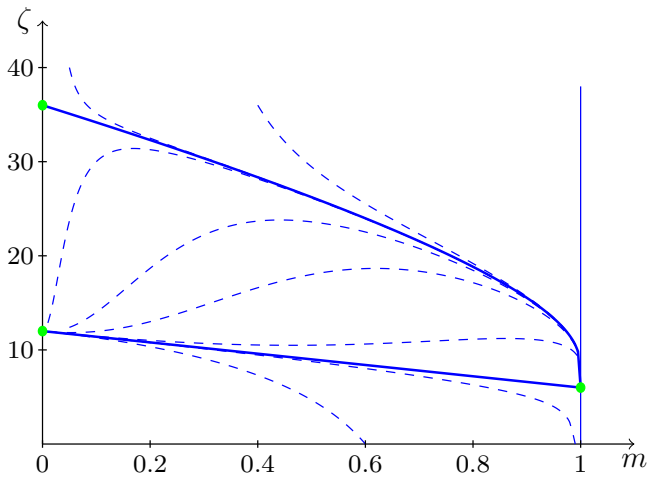

FIG. 3. Integral curves of Eq. (42). The separatices are depicted as solid thick lines. The dots are the singular points (43).

Eq. (42) suggests that the separatrix joining the singular points (0,12) and (1,6) is a straight line

$$\zeta = 6(2-m), \tag{44}$$

which, after returning to the variables R_1, R_2, and z, leads to the assumption that the system (38) admits the following integral:

$$R_1 + R_2 = \tfrac{1}{6}z. \tag{45}$$

A direct check shows that indeed $d(R_1+R_2)/dz = 1/6$ under the condition (45), so that this assumption is proved. The integral curves beginning in vicinity of this separatrix are attracted to it when m decreases, so one can expect that just this separatrix realizes the self-similar regime of the DSW near its soliton edge.

To determine the dependence of m on z, we find, with the use of Eqs. (38),

$$\frac{dm}{dz} = \frac{6\zeta(m)(1-m)(V_2(m)-V_1(m))}{z[\zeta(m)-3V_1(m)][\zeta(m)-3V_2(m)]}. \tag{46}$$

Substituting Eq. (44) and the expressions (40) in the above, we get the following equation:

$$\frac{dm}{dz} = -\frac{2-m}{zmK(m)}F(m), \tag{47}$$

where

$$F(m) = (2-m)E(m) - 2(1-m)K(m). \tag{48}$$

The solution of this equation determines $m = m(z)$ along the separatrix.

The form of expression (48) suggests that it can be obtained as a result of the calculation of some elliptic integral in which the integration limits may play the role of more convenient variables. Inspection of tables of such integrals shows that the formula 3.155.9 in Ref. [30] (which we write down here with notations slightly different from the original reference),

$$I = 3\int_{q_2}^{q_1} \sqrt{(q_1^2-y^2)(y^2-q_2^2)}\,dy$$
$$= q_1\big[(q_1^2+q_2^2)E(m) - 2q_2^2K(m)\big], \tag{49}$$

has the necessary structure. In Eq. (49) one has $q_1 > q_2 > 0$ and $m = 1-(q_2/q_1)^2$.

To establish the link between the two expressions (48) and (49), it is enough to take

$$q_1^2 + q_2^2 = 1, \tag{50}$$

so that $1-m = q_2^2/q_1^2$, $2-m = 1/q_1^2$. Assuming that the variables q_1, q_2 satisfy (50), we obtain

$$q_1^2 = \frac{1}{2-m}, \qquad q_2^2 = \frac{1-m}{2-m}, \tag{51}$$

and then, imposing $m = m$, we get $F(m) = (2-m)^{3/2}I$.

Since $dq_1/dm = q_1^3/2$, Eq. (47) can be cast under the form

$$\frac{dq_1}{d\ln(-z)} = -\frac{q_1}{2mK(m)}F(m), \tag{52}$$

which is more convenient for further calculations. On the other hand, the integral (49) with account of Eqs. (51) simplifies to

$$I = q_1\big[E(m) - 2\big(1-q_1^2\big)K(m)\big],$$

and its differentiation with respect to q_1 gives

$$\frac{dI}{dq_1} = 3q_1^2mK(m). \tag{53}$$

With the help of the formulas obtained we transform Eq. (52) to

$$\frac{dI}{I} = -\frac{3}{2}d\ln(-z).$$

Then, integration of this equation with the boundary condition $z = z_1$ at $m = 1$ yields z as a function of m:

$$z = z_1\,I^{-2/3}(m) = z_1\,\frac{2-m}{F^{2/3}(m)}, \tag{54}$$

where

$$z_1 = \frac{x_R(t)}{t^{1/3}} = -6(\mathcal{A}/4)^{2/3} \tag{55}$$

is the value of z for $m = 1$ (at the soliton edge of the DSW, see Sec. III).

From the formulas (39) and (51) we find the relationship between the R_i's and the q_i's:

$$R_1 = \frac{q_1^2}{6}z, \quad R_2 = \frac{q_2^2}{6}z, \tag{56}$$

so that for the dependence of the Riemann invariants on m we obtain:

$$R_1(m) = \frac{z_1}{6(2-m)I^{3/2}},$$
$$R_2(m) = \frac{(1-m)z_1}{6(2-m)I^{3/2}}. \tag{57}$$

Formulas (54), (55), and (57), together with Eq. (37), completely determine the self-similar solution of the Whitham equations: For fixed t we have $x(m) = t^{1/3}z(m)$, so that all functions are defined parametrically, with m playing the role of the parameter. Up to notations, this solution coincides with the one obtained in Ref. [9] by means of an asymptotic study of a Riemann-Hilbert problem in the framework of the inverse scattering transform method.

In the harmonic limit $m \ll 1$, the relation (54) reads

$$m = m_1 z^{-3/4}, \quad \text{where} \quad m_1 = \frac{2^{11/4}}{\sqrt{3\pi}}(-z_1)^{3/4}, \tag{58}$$

which leads to the expressions

$$r_1 = \frac{x}{12t} - \frac{m_1}{24}\frac{(-x)^{1/4}}{t^{3/4}}, \quad r_2 = \frac{x}{12t} + \frac{m_1}{24}\frac{(-x)^{1/4}}{t^{3/4}}. \tag{59}$$

It is important to notice that the difference $r_2 - r_1$, that is, the amplitude of the oscillations in the "quasilinear" region of Zakharov and Manakov [7], increases with growing distance from the soliton edge [as $(-x)^{1/4}$] but $r_2/r_1 \to 1$ and $m \to 0$ here. Hence, this limit is not a small-amplitude one and therefore the self-similar regime cannot be realized along the whole DSW; it takes place close enough to the soliton edge only; see Figs. 6(e), 6(f), and 8. Consequently, we have to turn to the general solution of the Whitham equations to obtain a full description of the DSW.

V. GENERAL SOLUTION

In this section, following Ref. [22], we turn to the general solution of the Whitham equations given by the formulas of Sec. II C. Our task now is to express the functions $W_i(r_1, r_2)$, $i = 1, 2$, in terms of the initial form $u_0(x)$ of the pulse. As was indicated above, at the first stage of evolution the DSW is located inside the region A and after the moment $t_{A/B}$ [see Eq. (32)] a second stage begins where it also reaches region B. Correspondingly, the expressions for W_i and $\mathscr{W}$ are given by different formulas and should be considered separately.

A. Solution in region A

In region A one can follow the procedure explained in Ref. [25]. One imposes the matching of the right edge of the DSW with the dispersionless solution (5): Just at $x = x_R(t)$, we have $r_1 = r(x, t)$, where $r(x, t)$ is the solution of (4), and $v_1(r_1, 0) = 6r_1$ [this follows from Eq. (19)]. Comparing in this case Eqs. (5) and (21) one obtains

$$W_1^{A}(r_1, 0) = w^{A}(r_1), \tag{60}$$

which embodies the same information as Eq. (20a). In terms of $\mathscr{W}$ this corresponds to the equation

$$\mathscr{W}^{A}(r_1, 0) + 2r_1\,\partial_1\mathscr{W}^{A}(r_1, 0) = w^{A}(r_1), \tag{61}$$

whose solution is

$$\mathscr{W}^{A}(r_1, 0) = \frac{1}{2\sqrt{-r_1}}\int_{r_1}^{0}\frac{w^{A}(\rho)\,d\rho}{\sqrt{-\rho}}. \tag{62}$$

This will serve as a boundary condition for the Euler-Poisson equation (24) whose general solution has been given by Eisenhart [32] in the form

$$\mathscr{W}^{A}(r_1, r_2) = \int_{r_1}^{0}\frac{\varphi^{A}(\mu)\,d\mu}{\sqrt{(\mu - r_1)|r_2 - \mu|}} + \int_{r_2}^{0}\frac{\psi^{A}(\mu)\,d\mu}{\sqrt{(\mu - r_1)(\mu - r_2)}}, \tag{63}$$

where the functions φ^{A} and ψ^{A} are arbitrary functions to be determined from the appropriate boundary conditions. By taking $r_2 = 0$ in this expression one sees that $\varphi^{A}(\mu)/\sqrt{-\mu}$ is the Abel transform of $\mathscr{W}^{A}(r_1, 0)$. The inverse transform reads [33]

$$\frac{\varphi^{A}(\mu)}{\sqrt{-\mu}} = -\frac{1}{\pi}\frac{d}{d\mu}\int_{\mu}^{0}\frac{\mathscr{W}^{A}(r, 0)\,dr}{\sqrt{r - \mu}}. \tag{64}$$

Plugging expression (62) for $\mathscr{W}^{A}(r, 0)$ in this formula and changing the order of integration, one obtains

$$\varphi^{A}(\mu) = \frac{1}{2\pi\sqrt{-\mu}}\int_{\mu}^{0}\frac{w^{A}(\rho)\,d\rho}{\sqrt{\rho - \mu}}. \tag{65}$$

For the initial profile (6), w^{A} is given in Eq. (7) and one gets explicitly

$$\varphi^{A}(\mu) = -\frac{x_0}{4\pi}\left(3 + \frac{1+\mu}{\sqrt{-\mu}}\tanh^{-1}\sqrt{-\mu}\right).$$

In order to determine the function ψ^{A}, one considers the left boundary of the DSW where, according to (20b), r_1 and r_2 are asymptotically close to each other. Let us write $r_1 = r$ and $r_2 = r + \epsilon$ with $r \in [-1, 0]$ and ϵ small and positive. One gets from (63)

$$\mathscr{W}^{A}(r, r+\epsilon) = \int_{r+\epsilon}^{0} d\mu\,\frac{\varphi^{A}(\mu) + \psi^{A}(\mu)}{\sqrt{(\mu - r)(\mu - r - \epsilon)}} + \int_{r}^{r+\epsilon}\frac{\varphi^{A}(\mu)\,d\mu}{\sqrt{(\mu - r)(r + \epsilon - \mu)}}. \tag{66}$$

In the right-hand side of the above equality, the second term converges when ϵ tends to 0 [toward $\pi\varphi^{A}(r)$], whereas the first one diverges unless $\varphi^{A}(r) + \psi^{A}(r) = 0$, this being true for all $r \in [-1, 0]$. This imposes that the functions φ^{A} and ψ^{A} should be opposite one the other and the final form of the Eisenhart solution in case A thus reads

$$\mathscr{W}^{A}(r_1, r_2) = \int_{r_1}^{r_2}\frac{\varphi^{A}(\mu)\,d\mu}{\sqrt{(\mu - r_1)(r_2 - \mu)}}, \tag{67}$$

where φ^{A} is given by formula (65).

B. Solution in region B

One looks for a solution of the Euler-Poisson equation in region B of the form

$$\mathscr{W}^{B}(r_1, r_2) = \mathscr{W}^{A}(r_1, r_2) + \int_{-1}^{r_1}\frac{\varphi^{B}(\mu)\,d\mu}{\sqrt{(r_1 - \mu)(r_2 - \mu)}}. \tag{68}$$

Indeed, this ensures that $\mathscr{W}^{B}$, (i) being the sum of two solutions of the Euler-Poisson equation is also a solution of this equation and (ii) verifies the boundary condition (25) since the second term of the right-hand side of (68) vanishes when $r_1 = -1$.

At the right boundary of the DSW, $\mathscr{W}^{B}(r_1, 0)$ verifies the same equation (61) as $\mathscr{W}^{A}(r_1, 0)$ does, where all the superscripts A should be replaced by B. The solution with the appropriate integration constant reads

$$\mathscr{W}^{B}(r_1, 0) = \frac{1}{2\sqrt{-r_1}}\int_{r_1}^{-1}\frac{w^{B}(\rho)\,d\rho}{\sqrt{-\rho}} + \frac{1}{2\sqrt{-r_1}}\int_{-1}^{0}\frac{w^{A}(\rho)\,d\rho}{\sqrt{-\rho}}. \tag{69}$$

The same procedure than the one previously used in part A of the DSW leads here to

$$\varphi^{\mathrm{B}}(\mu) = \frac{1}{2\pi\sqrt{-\mu}} \int_{-1}^{\mu} d\rho \, \frac{w^{\mathrm{A}}(\rho) - w^{\mathrm{B}}(\rho)}{\sqrt{\mu - \rho}}. \tag{70}$$

For the initial profile (6) one gets explicitly

$$\varphi^{\mathrm{B}}(\mu) = -\frac{x_0}{4} \frac{1+\mu}{\sqrt{-\mu}}.$$

In the generic case, Eqs. (68) and (70) give the solution of the Euler-Poisson equation in region B.

C. Characteristics of the DSW at its edges

It is important to determine the boundaries $x_{\mathrm{R}}(t)$ and $x_{\mathrm{L}}(t)$ of the DSW, as well as the values of the Riemann invariants r_1 and r_2 at these points. The law of motion of the soliton edge was already found in Sec. III and it is instructive to show how this result can be obtained from the general solution.

At the soliton edge we have $r_2 = r_3 = 0$ and $r_1 = r_{\mathrm{R}}(t)$. The corresponding Whitham velocities are $v_1 = 6\,r_{\mathrm{R}}$ and $v_2 = 2\,r_{\mathrm{R}}$ [see Eqs. (19)], and the two equations (21) read

$$\begin{aligned} x_{\mathrm{R}} - 6 r_{\mathrm{R}} t &= W_1(r_{\mathrm{R}}, 0) = w(r_{\mathrm{R}}), \\ x_{\mathrm{R}} - 2 r_{\mathrm{R}} t &= W_2(r_{\mathrm{R}}, 0) = \mathscr{W}(r_{\mathrm{R}}, 0). \end{aligned} \tag{71}$$

These formulas apply to both stages of evolution and therefore the superscripts A and B are dropped out. They give at once

$$\begin{aligned} t(r_{\mathrm{R}}) &= \frac{1}{4 r_{\mathrm{R}}} [\mathscr{W}(r_{\mathrm{R}}, 0) - w(r_{\mathrm{R}})], \\ x_{\mathrm{R}}(r_{\mathrm{R}}) &= \frac{1}{2} [3\mathscr{W}(r_{\mathrm{R}}, 0) - w(r_{\mathrm{R}})]. \end{aligned} \tag{72}$$

Let us consider the stage A, for instance. Equation (62) yields

$$\mathscr{W}^{\mathrm{A}}(r_{\mathrm{R}}, 0) = -\frac{1}{2\sqrt{r_{\mathrm{R}}}} \int_0^{r_{\mathrm{R}}} \frac{w^{\mathrm{A}}(\rho) d\rho}{\sqrt{-\rho}},$$

which, inserted into Eqs. (72), gives immediately the results (30) and (31). For instance, for the initial profile (6), when the right boundary is still in region A, one obtains explicitly

$$t(r_{\mathrm{R}}) = \frac{x_0}{16\, r_{\mathrm{R}}} \left(\sqrt{1 + r_{\mathrm{R}}} - \frac{\arcsin \sqrt{-r_{\mathrm{R}}}}{\sqrt{-r_{\mathrm{R}}}} \right). \tag{73}$$

At the wave-breaking time, $r_{\mathrm{R}} = 0$ and this yields $t_{\mathrm{WB}} = t(r_{\mathrm{R}} = 0) = x_0/24$ as already obtained [cf. Eq. (8)]. Stage A ends at time $t_{\mathrm{A/B}}$ at which the minimum (-1) of the smooth part of the profile enters the DSW. This corresponds to $t_{\mathrm{A/B}} = t(r_{\mathrm{R}} = -1)$ and yields, for the initial parabolic profile (6), $t_{\mathrm{A/B}} = \pi\, x_0/32$.

Let us now turn to the determination of the location $x_{\mathrm{L}}(t)$ of the left boundary of the DSW and of the common value $r_{\mathrm{L}}(t)$ of r_1 and r_2 at this point. In the typical situation the left boundary is located in region A. In this case the equations (21) for $i = 1$ and 2 are equivalent and read

$$x_{\mathrm{L}} - 12\, r_{\mathrm{L}} t = W_1^{\mathrm{A}}(r_{\mathrm{L}}, r_{\mathrm{L}}). \tag{74}$$

An equation for r_{L} alone is obtained by demanding that the velocity dx_{L}/dt of the left boundary is equal to the common value $12\, r_{\mathrm{L}}$ of v_1 and v_2 at this point [cf. Eqs. (17)]. The time derivative of Eq. (74) then yields

$$t = -\frac{1}{12} \frac{dW_1^{\mathrm{A}}(r_{\mathrm{L}}, r_{\mathrm{L}})}{dr_{\mathrm{L}}}. \tag{75}$$

Once $r_{\mathrm{L}}(t)$ has been determined by solving this equation, $x_{\mathrm{L}}(t)$ is given by Eq. (74).

Note that the relation $dx_{\mathrm{L}}/dt = 12\, r_{\mathrm{L}}$ is a consequence of the general statement that the small-amplitude edge of the DSW propagates with the group velocity corresponding to the wave number determined by the solution of the Whitham equations. Indeed, the KdV group velocity of a linear wave with wave-vector k moving over a zero background is $v_g = -3k^2$, and here $k = 2\pi/L = 2\sqrt{-r_{\mathrm{L}}}$ [cf. Eq. (12)], hence $v_g = 12\, r_{\mathrm{L}} = dx_{\mathrm{L}}/dt$, as it should. This property of the small-amplitude edge is especially important in the theory of DSWs for nonintegrable equations (see Refs. [34,35]).

We also study below a case different from (6) for which the left boundary of the DSW belongs to region B and corresponds to $r_1 = r_2 = -1$ [in the so-called triangular case corresponding to $u_0(x)$ given by Eq. (77)]. Then, at the small-amplitude edge $v_1 = v_2 = -12$ and Eqs. (21) yield $x_{\mathrm{L}} + 12 \cdot t = C^{\mathrm{st}}$, the constant being the common value of $W_1^{\mathrm{B}}(-1, -1)$ and $W_2^{\mathrm{B}}(-1, -1)$. It can be determined at $t = t_{\mathrm{WB}}$, leading in this case to

$$x_{\mathrm{L}} = -x_0 - 12(t - t_{\mathrm{WB}}). \tag{76}$$

It is worth noticing that the velocity $dx_{\mathrm{L}}/dt = -12$ agrees with the leading term in Eq. (59) for $r_1 = -1$ in spite of a nonvanishing amplitude of the self-similar solution in this limit. For a more detailed study of the small-amplitude region beyond the Whitham approximation, see, e.g., Ref. [12].

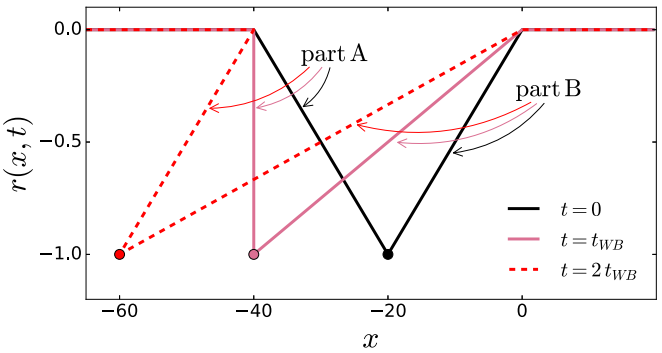

FIG. 4. Dispersionless evolution of the initial triangular profile (77) with $x_0 = 40$. The solid black, solid pink, and dashed red lines represent $r(x, t)$ solution of (4) for times $t = 0$, $t = t_{\mathrm{WB}}$ and $t = 2\, t_{\mathrm{WB}}$.

D. The global picture

We now compare the results of the Whitham approach with the numerical solution of the KdV equation for the initial profile (6) and also for a profile

$$u_0(x) = \begin{cases} -1 + \left| \frac{2x}{x_0} + 1 \right| & \text{for} \quad -x_0 \leqslant x \leqslant 0, \\ 0 & \text{elsewhere.} \end{cases} \tag{77}$$

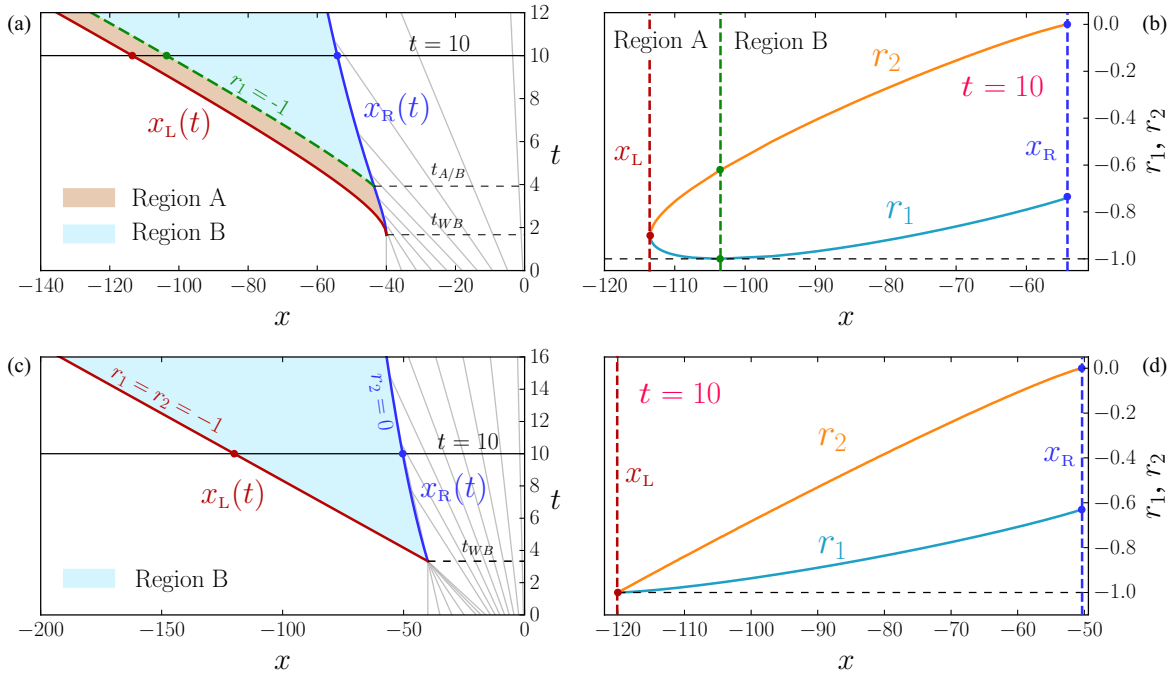

FIG. 5. The upper plots (a) and (b) refer to the parabolic initial profile, and the lower ones (c) and (d) to the triangular initial profile. Left column: Different regions in the (x, t) plane. The DSW occurs in the colored regions. The characteristics of the dispersionless evolution are represented as gray lines. In plot (a) the time $t_{A/B}$ is the time where part A of the initial profile has been completely absorbed by the DSW. For the triangular profile in plot (c) one has $t_{A/B} = t_{WB}$. Right column: Plot of the two varying Riemann invariants $r_1(x, t)$ and $r_2(x, t)$ at fixed $t = 10$ for $x_L(t) \leqslant x \leqslant x_R(t)$. In plots (a) and (b) the green dashed line marks the separation between regions A and B.

This profile is represented in Fig. 4 at $t = 0$, at wave-breaking time, which in the present case is equal to $t_{WB} = x_0/12$ and also at $t = 2\,t_{WB}$ (using the dispersionless approximation presented in Sec. II A).

We henceforth denote the initial profile (6) as "parabolic" and the initial profile (77) as "triangular." As was indicated above, the triangular profile has the particularity of having a DSW within the region B only. This is clear from Fig. 4: Part A of the initial profile does not penetrate into the DSW region before part B does. Or, phrasing this differently, according to the dispersionless evolution, at $t = t_{WB}$ both parts A and B penetrate into the region of multivaluedness at $x \leqslant -x_0$.

The DSW is described by Whitham method as explained in Secs. II B and II C. For this purpose one needs to determine r_1 and r_2 as functions of x and t ($r_3 \equiv 0$). This is performed as follows:

(i) First, we pick up a given $r_1 \in [-1,\ r_R]$, where r_R is the value of r_1 at the soliton edge, the point where the DSW is connected to the rarefaction wave (how to compute it has been explained in Sec. V C).

(ii) Second, at fixed t and r_1, we find the corresponding value r_2 as a solution of the difference equation obtained from Eqs. (21),

$$(v_1 - v_2) \cdot t = W_2(r_1, r_2) - W_1(r_1, r_2)\,, \tag{78}$$

where W_1 and W_2 are computed from Eq. (23).

(iii) Last, the corresponding value of x is determined by $x = W_1 + v_1 t$ (or, equivalently, $x = W_2 + v_2 t$).

This procedure gives, for each $r_1 \in [-1,\ r_R]$ and t, the value of r_2 and x. In practice, it makes it possible to associate to each (x, t) a couple (r_1, r_2). The result is shown in Figs. 5 for the two initial profiles (6) and (77).

Note that the characteristics of the DSW are different for the initial profiles (6) and (77): For the parabolic profile, in Fig. 5(a), the edge point of the DSW—at (x_0, t_{WB})—pertains to region A and corresponds to $r_1 = 0$, while for the triangular profile, in Fig. 5(b), the edge point of the DSW belongs to region B, with $r_1 = -1$. For the parabolic profile, the value $r_1 = -1$ defines a line which separates the regions A and B of the plane (x, t), see Fig. 5(a). This line reaches a boundary of the DSW only at $x_R(t_{A/B})$, where $t_{A/B}$ is the time where part A of the initial profile has just been completely absorbed within the DSW. On the other hand, for the triangular profile, the whole left boundary of the DSW corresponds to the line $r_1 = -1$, see Fig. 5(c).

The knowledge of $r_1(x, t)$ and $r_2(x, t)$ makes it possible to determine, for each time $t > t_{WB}$, $u(x, t)$ as given by the Whitham approach, for all $x \in \mathbb{R}$:

(i) In the regions $x \geqslant 0$ and $x \leqslant x_L(t)$, we have $u(x, t) = 0$.

(ii) In the region $[x_R(t), 0]$, one has $u(x, t) = r(x, t)$ which is solution of the Hopf equation (obtained by the method of characteristics, as explained in Sec. II A).

(iii) Inside the DSW, for $x \in [x_L(t), x_R(t)]$, the function $u(x, t)$ is given by expression (9), with $r_3 = 0$ and r_1 and r_2 determined as functions of x and t by the procedure just explained.

The corresponding profiles are shown in Fig. 6 for the parabolic and triangular initial distributions. The agreement with the numerical solution of Eq. (2) is excellent in both cases. The numerical simulations are performed using a

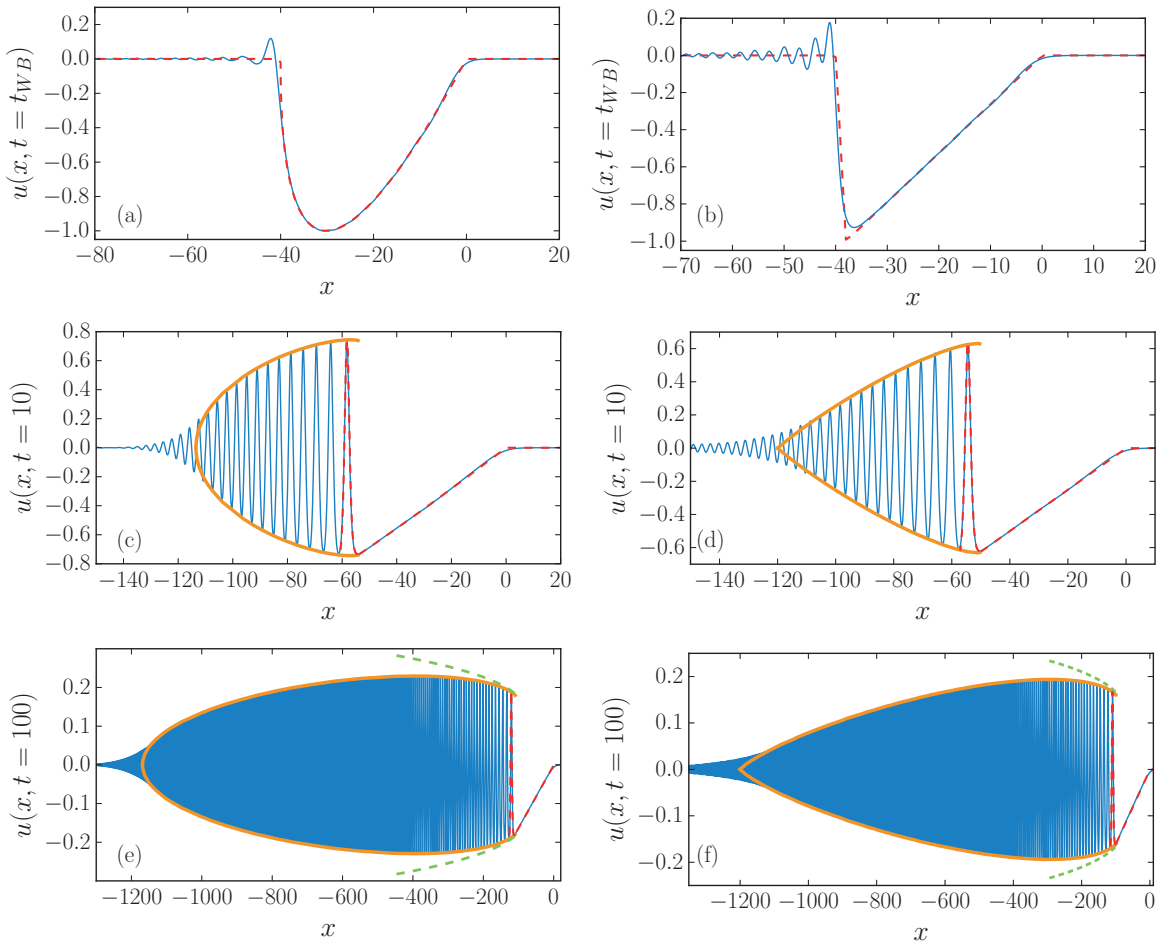

FIG. 6. $u(x,t)$ as a function of x for fixed t. The left column refers to the parabolic initial profile and the right one to the triangular initial profile. The upper row [(a) and (b)] corresponds to the wave-breaking time t_{WB}, the central row [(c) and (d)] to $t = 10$, and the lower one [(e) and (f)] to $t = 100$. The blue solid line corresponds to the numerical solution of Eq. (2). The thick envelopes correspond to the results of Whitham modulation theory. The dashed red lines represent the dispersionless profile $r(x,t)$ and also, in (c)–(f), the Whitham result for the soliton at the large-amplitude boundary of the DSW. The green dashed envelopes in (e) and (f) are the asymptotic self-similar results obtained in Sec. IV.

spatial mesh $h = 0.1$, evaluating the spatial derivatives u_x and u_{xxx} by means of, respectively, two- and four-point formulas (i.e., with an accuracy h^2), and time propagated using a fourth-order Runge-Kutta method with a time step $\Delta t = 10^{-3}$.

In Fig. 7 we also compare the wavelength of the nonlinear oscillations within the DSW as determined by Whitham approach [Eq. (12)] with the results of numerical simulations, and the agreement is again very good.

E. The initial square profile

In this section we discuss another type of initial condition, which we denote as a "square profile":

$$u_0(x) = \begin{cases} -1 & \text{for} \quad -x_0 \leqslant x \leqslant 0, \\ 0 & \text{elsewhere.} \end{cases} \tag{79}$$

El and Grimshaw already theoretically studied the same initial condition by using the method just explained [36]. We will here compare the theory with numerical simulations to indicate some limitations of the one-phase Whitham method which we use in the present work.

For this initial profile, wave breaking occurs instantaneously (i.e., $t_{\mathrm{WB}} = 0$), and until $t = x_0/4$ a plateau (i.e., a segment with constant $u(x,t) = -1$) separates the DSW (at the right) from a rarefaction wave (at the left). In this configuration, the DSW corresponds to the standard Gurevich-Pitaevskii scheme for a steplike initial profile with a single varying Riemann invariant (r_2 in this case). This DSW can be described using the self-similar variable $\zeta = (x + x_0)/t$; in this case Eq. (13) for $i = 2$ reads $\zeta = v_2(-1, r_2)$. One also obtains $x_{\mathrm{L}}(t) = -x_0 - 2t$, $x_{\mathrm{R}}(t) = -6t$ and the rarefaction wave corresponds to $r(x,t) = x/6t$ for $x \in [x_{\mathrm{R}}(t), 0]$.

It is interesting to remark that the Gurevich-Pitaevskii DSW can also be described within the approach exposed in Secs. II C and V D by solving Eq. (21) for $i = 2$. Here W_2^{A} should be computed from

$$\mathscr{W}^{\mathrm{A}}(r_1, r_2) = -x_0 \tag{80}$$

by means of Eq. (23). The form (80) of $\mathscr{W}^{\mathrm{A}}$ comes from (67) with $w^{\mathrm{A}}(r) = -x_0$.

At $t = x_0/4$ the plateau disappears, and one enters into region B with now, as usual, two varying Riemann invariants.

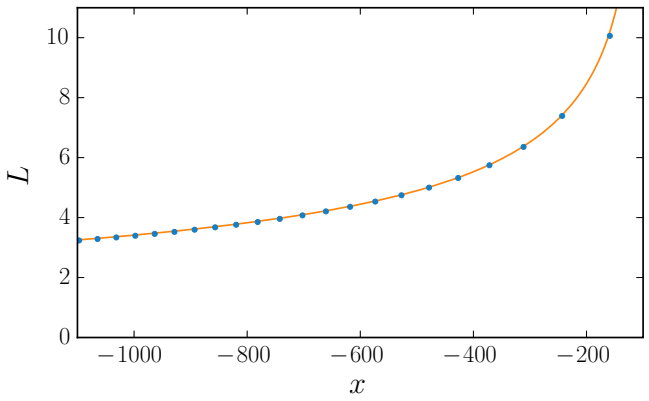

FIG. 7. Evolution of the wavelength of the nonlinear oscillations within the DSW as a function of position x. The figure corresponds to the time evolution of the parabolic initial profile represented in the lower left plot of Fig. 6 ($t = 100$). The continuous line represents the results of Whitham theory and the points are the value of the wavelength extracted from the numerical simulations.

Formulas (68) and (70) lead here to

$$\mathscr{W}^{\mathrm{B}}(r_1, r_2) = -x_0 - \frac{x_0}{\pi}\int_{-1}^{r_1} \frac{\sqrt{\mu+1}\, d\mu}{\sqrt{-\mu(r_1-\mu)(r_2-\mu)}},$$
$$= -x_0 + \frac{2\,x_0/\pi}{\sqrt{-r_1(1+r_2)}} \times\left\{\Pi\left(\frac{1+r_1}{r_1}, m\right) - K(m)\right\}, \tag{81}$$

where $m = (1 + 1/r_1)/(1 + 1/r_2)$ and Π is the complete elliptic integral of the third kind.

The predictions of Whitham theory are compared in Fig. 8 with numerical simulations. Surprisingly enough, the agreement between simulation and theory decreases at large time: At $t = 100$ one can notice oscillations in the envelope of the front part of the DSW (Gurevich-Pitaevskii part). Inspection of the dynamics of formation of the nonlinear structure reveals that, during the formation of the rear rarefaction wave, oscillations appear due to dispersive effects associated with the discontinuity of the initial condition (79): Their interference with the oscillations of the DSW leads to the modulated structure which can be observed in the lower plot of Fig. 8. Such a behavior requires a two-phase approach for a correct description. Note also that for numerical purposes the initial condition is smoothed[2] and that the beating phenomenon increases for sharper initial condition (or for lower values of x_0).

The predictions of the self-similar solution of Sec. IV are also displayed in Fig. 8. In this figure, the envelopes of the DSW expected from Eqs. (37) and (57) are represented by red dashed lines. In the vicinity of its soliton edge, the DSW is accurately described by the similarity solution. However this approach is not able to tackle the other, small-amplitude,

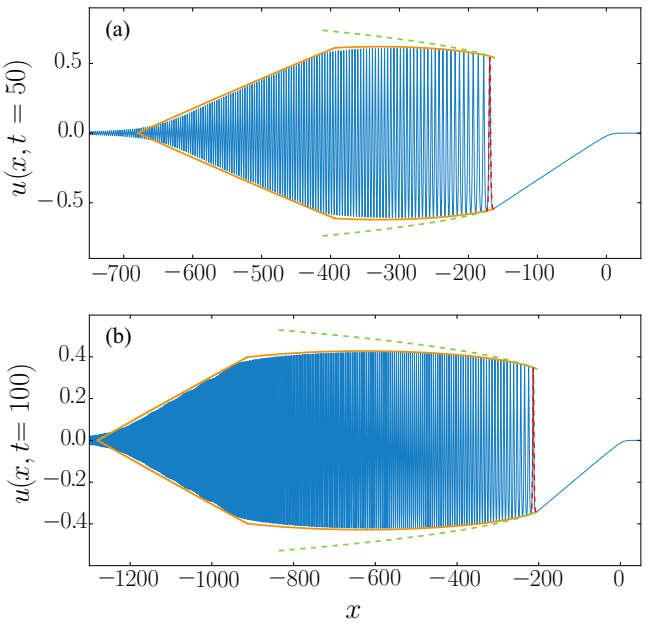

FIG. 8. Evolution of an initial square profile of type (79) with $x_0 = 80$ after a time $t = 50$ (a) and $t = 100$ (b). The blue solid lines are the results of numerical simulations. The orange envelopes are determined by Whitham method. The green dashed envelopes are the asymptotic self-similar results obtained in Sec. IV. The dashed red lines represent the Whitham result for the soliton at the large-amplitude boundary of the DSW. Note the change of scale in the axis of the two plots.

boundary of the shock. This is expected since—as discussed above—in the small-amplitude region a scaling different from the one of Eq. (3) holds, with the relevant self-similar parameter $\zeta = (x + x_0)/t$; see Refs. [9,37] for a general discussion.

VI. CONCLUSION

In the present work we have studied asymptotic solutions of the KdV equation for which no soliton is formed. We used the Whitham modulation theory combined with the generalized hodograph method for describing the DSW which is formed after wave breaking. The results typically compare very well with numerical simulations (see Sec. V D), except in the case of a initial square distribution (Sec. V E) where we argue that a two-phase approach would be needed for a correct description of the shock region.

A simple similarity description has been also obtained near the large-amplitude region of the shock, still within the framework of Whitham's approach. Our results confirm, simplify, and extend in some respects the previous works on this subject (see Sec. IV). We also showed in Sec. III that this theory provides a practical tool for the description of the nonlinear evolution of pulses and can be used for comparison with experimental data, since it yields simple analytic formulas for some characteristic features of DSWs. In particular our work reveals the existence of a conserved quantity which has remained unnoticed until now, see Eq. (36).

Extensions of the present approach to noncompletely integrable equations [35] and to other systems of physical interest are under study.

[2]In the numerical simulations presented in Fig. 8 we take $u_0(x) = \frac{1}{4}[\tanh(x/\Delta) - 1] \times \{1 + \tanh[(x + x_0)/\Delta]\}$ with $\Delta = 2$. This profile tends to (79) when $\Delta \to 0$.

ACKNOWLEDGMENTS

A.M.K. thanks Laboratoire de Physique Théorique et Modèles Statistiques (Université Paris-Saclay), where this work was started, for kind hospitality. This work was supported by the French ANR under Grant No. ANR-15-CE30-0017 (Haralab project).

[1] G. B. Whitham, *Linear and Nonlinear Waves* (Wiley Interscience, New York, 1974).
[2] V. I. Karpman, Phys. Lett. A **25**, 708 (1967).
[3] C. S. Gardner, J. M. Green, M. D. Kruskal, and R. M. Miura, Phys. Rev. Lett. **19**, 1095 (1967).
[4] I. A. Berezin and V. I. Karpman, Zh. Eksp. Teor. Fiz. **46**, 1880 (1964) [Sov. Phys. JETP **19**, 1265 (1964)].
[5] A. B. Shabat, Doklady AN SSSR **211**, 1310 (1973) [Sov. Mathem. Dokl. **14**, 1266 (1973)].
[6] M. J. Ablowitz and A. C. Newell, J. Math. Phys. **14**, 1277 (1973).
[7] V. E. Zakharov and S. V. Manakov, Zh. Eksp. Teor. Fiz. **71**, 203 (1976) [Sov. Phys. JETP **44**, 106 (1976)].
[8] M. J. Ablowitz and H. Segur, Stud. Appl. Math. **57**, 13 (1977).
[9] P. Deift, S. Venakides, and Z. Zhou, Commun. Pure Appl. Math. **47**, 199 (1994).
[10] G. A. El, A. L. Krylov, and S. Venakides, Commun. Pure Appl. Math. **54**, 1243 (2001).
[11] T. Claeys and T. Grava, Commun. Math. Phys. **286**, 979 (2009).
[12] T. Claeys and T. Grava, Commun. Pure Appl. Math. **63**, 203 (2010).
[13] J. L. Hammack and H. Segur, J. Fluid Mech. **65**, 289 (1974); **84**, 337 (1978).
[14] S. Trillo, M. Klein, G. F. Clauss, and M. Onorato, Physica D **333**, 276 (2016).
[15] A. M. Kamchatnov, A. Gammal, and R. A. Kraenkel, Phys. Rev. A **69**, 063605 (2004).
[16] M. A. Hoefer, M. J. Ablowitz, I. Coddington, E. A. Cornell, P. Engels, and V. Schweikhard, Phys. Rev. A **74**, 023623 (2006).
[17] W. Wan, S. Jia, and J. W. Fleischer, Nat. Phys. **3**, 46 (2007).
[18] G. Xu, M. Conforti, A. Kudlinski, A. Mussot, and S. Trillo, Phys. Rev. Lett. **118**, 254101 (2017).
[19] G. B. Whitham, Proc. R. Soc. A **283**, 238 (1965).
[20] A. V. Gurevich and L. P. Pitaevskii, Zh. Eksp. Teor. Fiz. **65**, 590 (1973) [Sov. Phys. JETP **38**, 291 (1974)].
[21] G. A. El and M. A. Hoefer, Physica D **333**, 11 (2016).
[22] G. A. El and V. V. Khodorovsky, Phys. Lett. A **182**, 49 (1993).
[23] A. V. Gurevich, A. L. Krylov, and N. G. Mazur, Zh. Eksp. Teor. Fiz. **95**, 1674 (1989) [Sov. Phys. JETP **68**, 966 (1989)].
[24] A. V. Gurevich, A. L. Krylov, and G. A. El, Pis'ma Zh. Eksp. Teor. Fiz. **54**, 104 (1991) [JETP Lett. **54**, 102 (1991)].
[25] A. V. Gurevich, A. L. Krylov, and G. A. El, Zh. Eksp. Teor. Fiz. **101**, 1797 (1992) [Sov. Phys. JETP **74**, 957 (1992)].
[26] A. L. Krylov, V. V. Khodorovskii, and G. A. El, Pis'ma Zh. Eksp. Teor. Fiz. **56**, 325 (1992) [JETP Lett. **56**, 323 (1992)].
[27] O. C. Wright, Commun. Pure Appl. Math. **46**, 423 (1993).
[28] F. R. Tian, Commun. Pure Appl. Math. **46**, 1093 (1993).
[29] A. M. Kamchatnov, *Nonlinear Periodic Waves and Their Modulations—An Introductory Course* (World Scientific, Singapore, 2000).
[30] I. S. Gradshteyn and I. M. Ryzhik, *Table of Integrals, Series, and Products* (Academic Press, New York, 1966).
[31] S. P. Tsarev, Math. USSR Izv. **37**, 397 (1991).
[32] L. P. Eisenhart, Ann. Math. **120**, 262 (1918).
[33] G. Arfken and H. J. Weber, *Mathematical Methods for Physicists* (Academic Press, Orlando, FL, 2005).
[34] G. A. El, Chaos **15**, 037103 (2005); **16**, 029901 (2006).
[35] A. M. Kamchatnov, Phys. Rev. E **99**, 012203 (2019).
[36] G. A. El and R. H. J. Grimshaw, Chaos **12**, 1015 (2002).
[37] H. Segur and M. J. Ablowitz, Physica D **3**, 165 (1981).